Metal-free scanning optical microscopy with a fractal fiber probe

C. M. Rollinson[1], S. M. Orbons[1], S. T. Huntington[1], B. C. Gibson[1]*, J. Canning[2], J. D. Love[3], A. Roberts[1] and D. N. Jamieson[1]

[1]*School of Physics, The University of Melbourne, Parkville, Victoria, 3010, Australia*
[2]*Interdisciplinary Photonics Laboratories (iPL), School of Chemistry, University of Sydney, Camperdown, Sydney, New South Wales, 2006, Australia*
[3]*Optical Sciences Group, RSPhysSE, The Australian National University, Canberra, Australian Capital Territory, 0200, Australia*
[*]*Corresponding author: b.gibson@unimelb.edu.au*

Abstract: Scanning Near-field Optical Microscopy (SNOM) is the leading instrument used to image optical fields on the nanometer scale. A metal-coating is typically applied to SNOM probes to define a subwavelength aperture and minimize optical leakage, but the presence of such coatings in the near field of the sample can often cause a substantial change in the sample emission properties. For the first time, the authors demonstrate near-field imaging on a metal substrate with a metal-free probe made from a novel structured optical fiber, designed to maximize optical throughput and potentially remove the need for the metal.

OCIS codes: (060.2280) Fiber design and fabrication; (060.4005) Microstructured fibers; (060.5295) Photonic crystal fibers; (180.4243) Near-field microscopy; (180.5810) Scanning microscopy; (060.2350) Fiber optics imaging; (050.1220) Apertures; (050.1940) Diffraction.

References and links

1. E. Betzig, J. K. Trautman, T. D. Harris, J. S. Weiner, and R. L. Kostelak, "Breaking the diffraction barrier: optical microscopy on a nanometric scale," Science **251**, 1468-1470 (1991).
2. J. Kim and K.-B. Song, "Recent progress of nano-technology with NSOM," Micron **38**, 409 (2007).
3. D. W. Pohl, "Optics at the nanometre scale," Philos. Trans. R. Soc. London Ser. A-Math. Phy. Engin. Scie. **362**, 701-717 (2004).
4. D. I. Kavaldjiev, R. Toledo-Crow, and M. Vaez-Iravani, "On the heating of the fiber tip in a near-field scanning optical microscope," Appl. Phys. Lett. **67**, 2771-2773 (1995).
5. N. E. Dickenson, E. S. Erickson, O. L. Mooren, and R. C. Dunn, "Characterization of power induced heating and damage in fiber optic probes for near-field scanning optical microscopy," Rev. Scie. Instrum. **78**, 53712/53711-53712/53716 (2007).
6. P. Hoffmann, B. Dutoit, and R. P. Salathe, "Comparison of mechanically drawn and protection layer chemically etched optical fiber tips," Ultramicroscopy **61**, 165-170 (1995).
7. P. Lambelet, A. Sayah, M. Pfeffer, C. Philipona, and F. Marquis-Weible, "Chemically etched fiber tips for near-field optical microscopy: a process for smoother tips," Appl. Opt. **37**, 7289-7292 (1998).
8. R. Stöckle, C. Fokas, V. Deckert, R. Zenobia, B. Sick, B. Hecht, and U. P. Wild, "High-quality near-field optical probes by tube etching," Appl. Phys. Lett. **75**, 160 (1999).
9. S. T. Huntington, B. C. Gibson, J. Canning, K. Digweed-Lyytikainen, J. D. Love, and V. Steblina, "A fractal-based fibre for ultra-high throughput optical probes," Opt. Express **15**, 2468-2475 (2007), http://www.opticsinfobase.org/oe/abstract.cfm?URI=oe-15-5-2468.
10. D. J. Shin, A. Chavez-Pirson, S. H. Kim, S. T. Jung, and Y. H. Lee, "Diffraction by a subwavelength-sized aperture in a metal plane," J. Opt. Soc. Am. A (Optics, Image Science and Vision) **18**, 1477-1486 (2001).
11. S. Kühn and V. Sandoghdar, "Modification of single molecule fluorescence by a scanning probe," Appl. Phys. B, Lasers Opt. (Germany) **B84**, 211-217 (2006).
12. F. Zenhausern, M. P. O'Boyle, and H. K. Wickramasinghe, "Apertureless near-field optical microscope," Appl. Phys. Lett. **65**, 1623-1625 (1994).
13. B. Knoll and F. Keilmann, "Near-field probing of vibrational absorption for chemical microscopy," Nature **399**, 134-137 (1999).
14. D. Courjon, K. Sarayeddine, and M. Spajer, "Scanning tunneling optical microscopy," Opt. Commun. **71**, 23-28 (1989).
15. R. C. Reddick, R. J. Warmack, D. W. Chilcott, S. L. Sharp, and T. L. Ferrell, "Photon scanning tunneling microscopy," Rev. Scie. Instrum. **61**, 3669-3677 (1990).

#105266 - $15.00 USD Received 12 Dec 2008; revised 18 Jan 2009; accepted 22 Jan 2009; published 29 Jan 2009

16. E. L. Buckland, P. J. Moyer, and M. A. Paesler, "Resolution in collection-mode scanning optical microscopy," J. Appl. Phys. **73**, 1018-1028 (1993).
17. V. Sandoghdar and S. Wegscheider, "Reflection scanning near-field optical microscopy with uncoated fiber tips: How good is the," J. Appl. Phys. **81**, 2499 (1997).
18. D. Courjon, J. M. Vigoureux, M. Spajer, K. Sarayeddine, and S. Leblanc, "External and internal reflection near field microscopy: experiments and results," Appl. Opt. **29**, 3734-3740 (1990).
19. J. Canning, E. Buckley, and K. Lyytikainen, "Propagation in air by field superposition of scattered light within a Fresnel fiber," Opt. Lett. **28**, 230-232 (2003).
20. V. R. Almeida, X. Qianfan, C. A. Barrios, and M. Lipson, "Guiding and confining light in void nanostructure," Opt. Lett. **29**, 1209-1211 (2004).
21. Q. Xu, V. R. Almeida, R. R. Panepucci, and M. Lipson, "Experimental demonstration of guiding and confining light in nanometer-size low-refractive-index material," Opt. Lett. **29**, 1626-1628 (2004).
22. M. A. Paesler and P. J. Moyer, *Near-field optics : theory, instrumentation, and applications* (Wiley, New York, 1996).
23. C. Martelli, J. Canning, B. C. Gibson, and S. T. Huntington, "Bend loss in structured optical fibres," Opt. Express **15**, 17639-17644 (2007).
24. P. B. Johnson and R. W. Christy, "Optical constants of the noble metals," Phys. Rev. B, Solid State **6**, 4370-4379 (1972).
25. M. Mansuripur, *Classical optics and its applications* (Cambridge University Press, Cambridge, 2002).
26. T. W. Ebbesen, H. J. Lezec, H. F. Ghaemi, T. Thio, and P. A. Wolff, "Extraordinary optical transmission through sub-wavelength hole arrays," Nature **391**, 667-669 (1998).
27. Y. Poujet, M. Roussey, J. Salvi, F. I. Baida, D. Van Labeke, A. Perentes, C. Santschi, and P. Hoffmann, "Super-transmission of light through subwavelength annular aperture arrays in metallic films: Spectral analysis and near-field optical images in the visible range," Photon. Nanostruct. Fundam. Appl. **4**, 47-53 (2006).
28. Y. Poujet, J. Salvi, F. I. Baida, D. Van Labeke, A. Perentes, C. Santschi, and P. Hoffmann, "Near-field optical images of subwavelength annular aperture arrays exhibiting an extraordinary transmission," J. Microsc. **229**, 203 (2008).
29. S. M. Orbons, D. Freeman, B. Luther-Davies, B. C. Gibson, S. T. Huntington, D. N. Jamieson, and A. Roberts, "Optical properties of silver composite metamaterials," Physica B-Condensed Matter **394**, 176-179 (2007).
30. S. T. Huntington and F. Ladouceur, "Evanescent fields - Direct measurement, modeling, and application," Microsc. Res. Techn. **70**, 181-185 (2007).
31. G. A. Valaskovic, M. Holton, and G. H. Morrison, "Parameter control, characterization, and optimization in the fabrication of optical fiber near-field probes," Appl. Opt. **34**, 1215-1228 (1995).

1. Introduction

Optical throughput is the major limitation preventing the advanced applicability of SNOM in fields such as high-speed nanoengineering processes, biomedical diagnostics and ultra-high density data storage. The technique generally employs metal-coated, tapered optical fibers possessing a subwavelength aperture to probe optical signals in the near-field of a sample [1-3]. Excessive losses occur as light passes through the subwavelength aperture and also as a result of the interaction of light with the metal-coating in the tapered region of the probe. These throughput limitations cannot be overcome by simply coupling more light into the probe, since the over-injection of power can cause thermal damage to the probe or sample [4, 5]. Etching techniques for large cone-angle probes [6-8] have been developed to improve throughput but can limit application to samples with relatively large topographical features due to the physical size of the probe. As a means to improve probe throughput by reducing the interaction between propagating light and the metal-coating, the novel fractal fiber has recently been reported to exhibit superior optical throughput over standard step-index and periodic structured fibers [9]. The capacity of the uncoated fractal fiber for use in metal-free scanning probe microscopy is compared in this work with standard fiber probes: one which is uncoated and another which is metal-coated.

In addition to throughput limitations, the metal-coating of apertured probes can limit application to metallic samples due to distortions induced by coupling between the probe and the sample surface [10]. Furthermore, the metal-coating can be problematic when characterizing the emission properties of molecules, since the close presence of metal leads to quenching of the emission due to the smearing of the levels and an increase in fast non-radiative decays [11]. The metal-coating also limits achievable resolutions with apertured

#105266 - $15.00 USD Received 12 Dec 2008; revised 18 Jan 2009; accepted 22 Jan 2009; published 29 Jan 2009

probes to approximately 20 nm for visible light applications due to the finite penetration depth of the metal [1-3]. It is also possible that the interaction between the metal-coating and a metallic sample surface can limit resolution by increasing the effective probe aperture size closer to that defined by the outer edges of the metal layers. The limitations of apertured probes have motivated the development of alternative probe designs such as apertureless scattering probes [12, 13] and tunneling probes for use in STOM [14] or PSTM [15].

Traditional SNOM achieves subwavelength resolution via the aperture at the tip of a metal-coated probe [1-3]. Numerical [16] and experimental [17] results have shown that the resolutions achievable with metal-free fiber tips is diffraction limited unless scattering is the dominant transduction mechanism. This is generally achieved in STOM/PSTM configurations where the sample is illuminated by total internal reflection so that only the evanescent tail is present in the near-field of the sample. Schemes which illuminate the sample, such that the near-field is dominated by propagating components, are ultimately diffraction limited when an uncoated probe is used. The demonstration of subwavelength resolution using uncoated tips in reflection mode SNOM [18] is reportedly a topography-induced effect and the optical resolution remains diffraction limited [17]. Illumination by total internal reflection is not always possible, especially for thick or opaque samples. Overcoming the diffraction limit without a metal-coating under normal illumination conditions poses ongoing challenges and will require an improved understanding of subwavelength field-localization at the dielectric air-interface of the probe [19-21]. In their present form, standard step-index fiber probes require metal-coatings to overcome the diffraction limit and enable subwavelength imaging.

Uncoated fiber probes have been used as apertureless probes in STOM/PSTM where scattering is the dominant mechanism for mode coupling into the probe [14, 15]. The scattering capture fraction is a function of the refractive index of the fiber probe or the NA [22]. Standard singlemode step-index optical fibers have low NAs and are poorly suited for use as near-field probes where scattering is the operative signal transduction mechanism. Fibers with a high probe NA such as the fractal fiber, therefore, hold potential for use in metal-free scattering SNOM with enhanced scattering capture fractions. The capacity of the uncoated fractal fiber for use in apertureless scanning probe microscopy of a metallic nano-structured sample is compared here with standard fiber probes: one which is uncoated and another which is coated with chromium and aluminium.

1.1 Light confinement by fractal fiber probes

An optical probe made from fractal fiber demonstrated a substantial increase in optical confinement and numerical aperture (NA) compared to probes made from a standard step-index fiber and a periodic photonic crystal fiber (PCF) [9]. Light was imaged as it exited the probes and caused fluorescence in a solution with a refractive index of ~1.461. The imaged intensity exiting the fractal fiber probe was much greater than the standard fiber probe demonstrating the enhanced probe throughput. When surrounded in air, the probe NAs are estimated as being approximately 0.14, 0.32 and 0.53 for the standard, periodic PCF and the fractal fiber probes, respectively. The results indicated that when the fractal probe is used as a source and is surrounded by air, optical confinement can be maintained to within ~1μm of the probe tip. The enhanced throughput and high probe NA has been attributed to the maintenance of the fiber structure along the taper [9]. The fractal fiber has also been shown to exhibit extremely low bend loss, offering a potential additional advantage over conventional fibers for commercial SNOM systems which typically employ bent probes. The low bend loss is attributed to the unique quasi-periodic distribution of air-holes in the silica cladding which spoils resonant coupling out of the core [23].

A microscope image of the fractal fiber end-face and a schematic representation of the taper cross-section are shown in Figs. 1(a) and (b), respectively. The fiber consists of three rings of holes whose cross-sectional area increases with distance from the center core region. Each inner ring of holes is rotated by π/n with respect to its neighboring ring, where n is the number of holes in each ring. As the fractal fiber is reduced in diameter along a taper, the modal field remains confined within the core region by a successive ring of holes as the inner

#105266 - $15.00 USD Received 12 Dec 2008; revised 18 Jan 2009; accepted 22 Jan 2009; published 29 Jan 2009

rings collapse. The average refractive index of the fiber decreases with increasing distance from the core and the radially variant interstitial regions spoil resonant coupling between each region, minimizing optical leakage and bend loss. The improved confinement of the fractal fiber has the potential to significantly reduce the length over which propagating light interacts with a metal-coating placed on the probe; thereby decreasing the associated losses and enhancing optical throughput. This paper presents the results of experiments which compare the imaging capacity of an uncoated fractal fiber probe with metal-coated and uncoated standard fiber probes in the application of a metallic nanostructured sample.

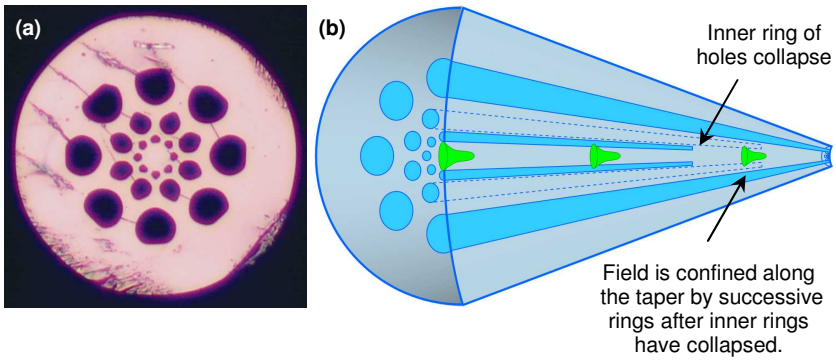

Fig. 1. (a) CCD image of the cleaved end-face of the fractal fiber (outer diameter of 125 μm) and (b) a schematic diagram illustrating how the fractal fiber design allows enhanced modal confinement along a taper: the inner ring of holes collapses into the core region and the modal field is then confined by the successive rings of holes.

2. Examination of a metallic nanostructure

The silver film sample under investigation in this work is shown in the scanning electron microscope (SEM) image in Fig. 2(a). The sample was fabricated by depositing a silver film of 105 nm thickness by thermal evaporation onto a glass substrate. The annular aperture array (AAA) was then etched into the silver film by focused ion beam (FIB) lithography and imaged using a FEI Nova Dualbeam™ FIB and SEM system. The structure consists of 500 nm outer diameter annular apertures, with inner diameters of 300 nm, arranged in a square array with periodicities of 1000 nm and 960 nm in the horizontal and vertical directions, respectively. Such a structure was selected since it combines spatial information of varying size: the locations of the apertures separated by approximately 1000 nm and the spatial detail of the apertures themselves which is of order 200 nm.

Finite Element Method (FEM) simulations incorporating the finite conductivity of silver [24] were employed to predict the transmission spectrum and near-field properties of the sample described above in the absence of a probe. The calculated transmission spectrum normalized to the incident field (not shown here) exhibits a peak transmission of ~50% at the localized aperture resonance at 1650 nm. Since the fiber probes tested in this work are not suited for operation with infrared light, a 532 nm laser was used in the imaging experiments described below which provided adequate transmission through the sample even though the computed transmission at this wavelength is of the order of only a few percent. The calculated magnitude of the electric field at a height of 5 nm above the sample for incident light polarized at 25° to the vertical axis (corresponding to the polarization direction of measurements) is shown in Fig. 2(d) for 1650 nm and in Fig. 2(e) for 532 nm. The choice of polarization direction was completely arbitrary. The simulated electric field distributions at the two wavelengths are similar to within measurement uncertainty of the field at 1650 nm. The field around the structure has a higher degree of complexity at 532 nm than at 1650 nm since the multiple diffracted orders produce a Talbot pattern [25] which is expected to affect what is measured using SNOM. Interestingly, the image in Fig. 2(e) provides more evidence

#105266 - $15.00 USD Received 12 Dec 2008; revised 18 Jan 2009; accepted 22 Jan 2009; published 29 Jan 2009

of evanescent surface waves at 532 nm due to interactions between apertures in the array [26], which is also expected to have a measurable effect on the fields imaged by SNOM probes. Although obtaining measurements at 532 nm leads to a more complex field pattern and much weaker transmission than with a smaller structure, it is shown that this does not affect our overall conclusions regarding the sensitivity of the probes. As a consequence, the sample examined should be regarded as a test object for the probes rather than the measurements revealing details of the electromagnetic structure surrounding the AAA.

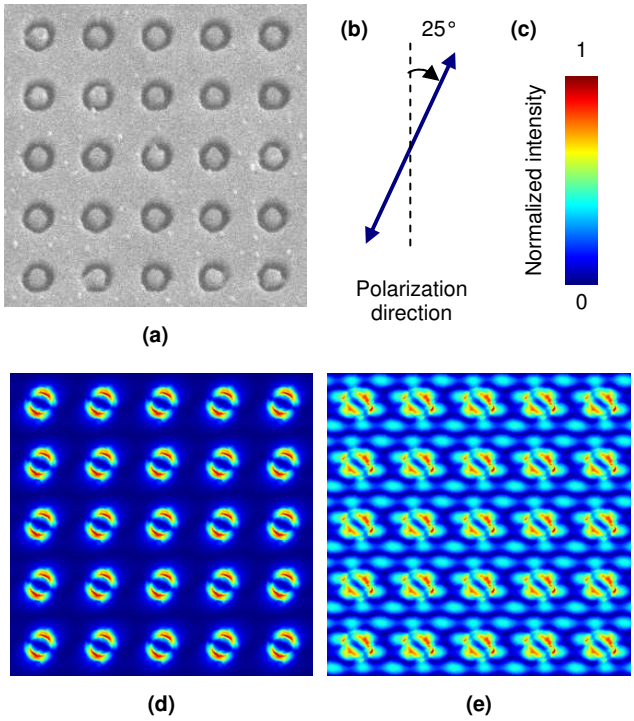

Fig. 2. (a) SEM image of a 5 × 5 µm section of the silver film sample. (b) The polarization direction for the simulated images in (d) and (e). (c) The normalized intensity scale for the simulated images ranges from dark blue to black corresponding to 0 and 1, respectively. The magnitude of the electric field simulated in the absence of a probe for a height of 5 nm above a 5 × 5 µm section with incident light at (b) 1650 nm and (c) 532 nm.

AAAs have shown themselves to present significant challenges to near-field characterization. Metal-free, fiber probes have been previously used in both reflection and collection mode SNOM to investigate the near-field properties of AAAs in thin silver films [27, 28]. However, the expected fields were not resolved experimentally which was attributed to the limitations of the dielectric probe. The authors concluded that metallized tips with smaller apertures are required to improve resolution. The use of metallic probes, however, seems an unlikely solution since in previous work it has been found that the interaction of the metal-coating on a probe with a metallic sample surface can lead to significant differences between the measured near-field intensity and that which exists in the absence of the probe [10]. This distortion is likely to be caused by the local field enhancement due to surface-plasmon effects which act to smear out any fine structure and modify near-field measurements. This was verified in recent work which investigated the near-field properties of AAAs on thin silver films using a cantilevered, metal-coated SNOM probe in collection mode with normal-force position control [29]. The expected fields were not clearly resolved and the measured profiles did not compare well with simulations. This was attributed firstly to the interaction between the metal-coating on the probe and the sample surface and secondly to

#105266 - $15.00 USD Received 12 Dec 2008; revised 18 Jan 2009; accepted 22 Jan 2009; published 29 Jan 2009

the oscillatory motion of the probe during image acquisition. The SNOM images were obtained after averaging over the full amplitude of the probe oscillation which affected the measured near-field profiles of the highly diffractive sample. This is consistent with recent work which has shown that the vertical oscillation of the probe in normal-force feedback loops can be disadvantageous to the detection efficiency [30].

As previously discussed, fibers with high probe NAs are better suited for application in metal-free probe microscopy due to enhanced scattering capture fractions over standard low NA fibers. Fractal fiber probes have enhanced throughput over standard fiber and a higher NA, suggesting that this type of probe may be useful for the imaging of metallic structures where the use of metallic probes has been problematic.

3. Experimental detail

SEM images of the three types of fiber probes used in this work are shown in Fig. 3. The straight, metal-coated probes were obtained from Nanonics Inc. and consisted of a fiber designed for singlemode operation at 488 nm, which was tapered and coated with chromium and aluminium to form a specified 50 nm aperture at the probe tip. The uncoated probes were fabricated at room temperature by a standard laser-based pulling technique [31] from samples of the fractal fiber and a standard step-index fiber designed for singlemode operation at 460 nm. No additional gas was used to pressurize the air-holes of the fractal fiber during tapering. Probes made from the standard and fractal fibers were coated with approximately 5 nm of carbon to enable acquisition of the SEM images in Figs. 3(b) and (c), respectively. These SEM images reveal similar tip geometries between the standard and fractal fiber probes which both have flat surfaces at the apex, consistent with cleaving under tension. The uncoated probes used in the imaging experiments described below were not coated with carbon and each had uniform taper profiles with approximate half-angles of 3°.

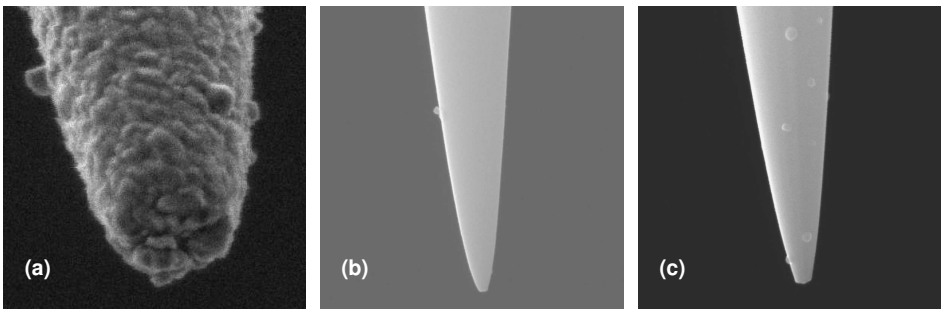

Fig. 3. SEM images of the three types of probes used in this work: (a) metal-coated standard fiber, (b) uncoated standard fiber and (c) uncoated fractal fiber. Each image is 2 × 2 μm in size.

The test probes were each mounted separately on a Physik Instrumente NanoCube® and scanned across the face of the silver film sample which was illuminated from the glass substrate side with a 532 nm laser beam. The incident light was polarized at (25 ± 5)° to the vertical axis of the sample and expanded with a defocused microscope objective. Light was collected by each probe, propagated along the fiber to a photomultiplier tube (PMT) and recorded with a PC which also controlled the probe translation via the NanoCube. A microscope, mounted above the sample and test probe, was used in alignment and positioning. The imaging sample comprised a 50 μm × 50 μm square array of annular apertures and each test probe was scanned across a unique section of the surface. Intensity maps were formed from the data recorded by the PMT as the probe was scanned across a 5 × 5 μm test region in 50 nm steps in both the horizontal and vertical planes at a distance of approximately 50 nm from the sample surface.

Each of the test probes was stepped closer in steps of 50 nm until the probe was observed to collide with the surface. From the images recorded after each step, the images which were measured just before collision were selected and consequently, the height of the probe was

#105266 - $15.00 USD Received 12 Dec 2008; revised 18 Jan 2009; accepted 22 Jan 2009; published 29 Jan 2009

estimated as being within 50 nm from the surface. A tilt in the sample would induce an uncertainty in the distance between the probe and sample over the 5 × 5 μm scan area. However, the measured images revealed relatively uniform intensity distributions over the scan area; indicating a minimal effect by any tilt in the sample. Commercial SNOM systems typically control the probe to sample distance by a normal-force feedback mechanism which requires oscillation of the probe and enables the recording of topographical information [2]. The test object is a highly diffractive sample and as such, the transmitted fields are expected to vary significantly over short ranges. As a result, the test probes were not oscillated in either a shear-force or normal-force configuration so that optical information could be collected on a point-to-point basis in one plane. The lack of probe oscillation avoided related distortions [29, 30] but prevented topographical images from being recorded.

4. Results

The raw intensity maps collected by each of the test probes are shown in Fig. 4. The size and period of the sample features imaged by the metal-coated probe (Fig. 4(a)) are consistent with the physical properties of the sample. However, the expected complex field distribution as in Fig. 2(e) was not resolved. The image measured by the metal-coated probe features spots which, although uniformly aligned, are not distinct. This is likely to be due to the complex fields expected to be present in the absence of the probe, shown in Fig. 2(e), as well as surface plasmon coupling between the probe and the surface as expected from previous work [10, 29]. Plasmon coupling between the metallic probe and the sample can affect resolution by increasing the effective probe aperture size closer to that defined by the outer edges of the metal layers. The image in Fig. 4(a) shows improved resolution compared to what was measured by a cantilevered, metal-coated SNOM probe with a similar silver film sample [29]. This is perhaps due to loss in resolution caused by the oscillatory motion of the probe which was controlled by normal-force feedback. A technique which does not oscillate the probe may avoid the detection efficiency issues associated with normal-force position control [29, 30] and enable improved resolution using a metal-coated probe.

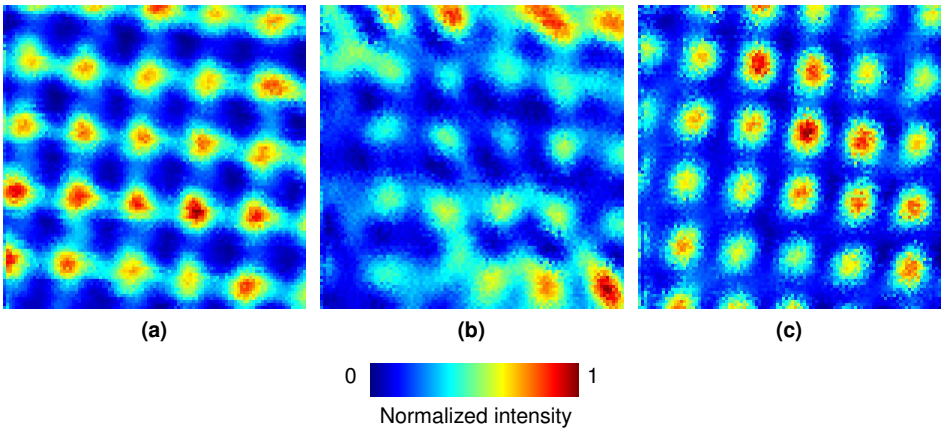

Fig. 4. Unprocessed intensity maps scanned in collection mode over 5 × 5 μm sections of the test sample by (a) the metal-coated probe, (b) the uncoated standard fiber probe and (c) the uncoated fractal fiber probe. The intensity scale used ranges from dark blue to black corresponding to 0 and 1, respectively.

The uncoated standard fiber probe was also unable to resolve the fields expected to be present above the sample as shown in Fig. 4(b). In previous work, the majority of the optical power in an uncoated standard fiber probe has been shown to leak at approximately 40 μm from the tip when used as a source and surrounded by a higher refractive index medium [9]. The poor resolution of the image measured by the uncoated standard fiber probe is expected to

#105266 - $15.00 USD Received 12 Dec 2008; revised 18 Jan 2009; accepted 22 Jan 2009; published 29 Jan 2009

be due to the effective collection aperture being too large, too complex and too far from the sample.

The image collected by the fractal fiber probe (Fig. 4(c)) resolves a uniformly aligned and distinct array of approximately 500 nm diameter spots which compare very well with the size and shape of the physical structure of the sample. The period of the features measured by the fractal fiber probe also compares very well with the expected pitch of 1 μm. A number of each of the standard and fractal fiber probes were tested in the imaging experiments and the images shown in Fig. 4(b) and (c) represent typical images obtained using the respective probes. The peak intensities recorded by the fractal probes were on average three times greater than those recorded by the uncoated standard fiber probes. The probes used in this work were chosen to have similar taper profiles and half-angles and it is believed that slight variations in the probe geometries have not contributed greatly to the differences in the images recorded using the three probes.

There is no obvious distortion arising from probe-sample interactions in the image measured by the fractal fiber probe. However, the expected complex field distribution as in Fig. 2(e) has not been resolved by the fractal probe. This is likely to be due firstly to the lack of accurate probe position control to maintain the probe at a constant height above the sample. Secondly, the lack of a defined aperture is likely to have prevented the detection of subwavelength features since the near-field of the sample is dominated by propagating components under normal illumination conditions. The resolution of subwavelength features may be achieved by illuminating the sample via total internal reflection so that the near-field contains only non-propagating, evanescent components, although obviously in the case of field characterization the fields would need to be calculated according to the precise excitation geometry.

5. Conclusions

A fractal fiber probe has been shown in previous work to exhibit enhanced optical throughput and an NA that is approximately four times larger than a standard fiber probe [9]. This fiber has also been shown to have extremely low bend loss [23] from which one would extrapolate lower taper losses in both straight and bent probes. The peak intensities collected by uncoated fractal probes were observed in this work to be on average three times larger than for uncoated standard fiber probes. This is consistent with previous work that reported enhanced probe throughput and much higher intensities at the tip of the fractal probe. The measured images reported in this paper demonstrate that the collection capability of an uncoated fractal fiber probe is far superior to an uncoated standard probe and is comparable, if not better than, a metal-coated probe. This is a significant result since the uncoated fractal fiber probe possesses no defined aperture, whereas the metal-coated probe is specified as having a 50 nm aperture. In addition, the metal-coated probe used in this work was unable to clearly distinguish the features in the metallic thin film sample, most likely due to surface plasmon coupling, which would effectively increase the probe aperture size closer to that defined by the outer edges of the metal layers.

The enhanced imaging performance of the uncoated fractal probe over the standard fiber probe can be directly attributed to the superior confinement and collection properties of the fiber. The lack of a metal-coating has avoided field distortions due to probe-sample interactions. It is expected that introducing probe-sample distance control and illuminating the sample by total internal reflection, as in a STOM/PSTM configuration, may enable the resolution of subwavelength features in such metallic nanostructures. Future designs like the fractal fiber, possessing more rings and more air-holes per ring, hold exciting potential for optimizing optical confinement in subwavelength structures. Such structures may be able to enhance scattering capture fractions and also move effective collection apertures even closer to the tip of tapered probes, potentially removing the need for a metal-coating altogether.

#105266 - $15.00 USD Received 12 Dec 2008; revised 18 Jan 2009; accepted 22 Jan 2009; published 29 Jan 2009

Acknowledgments

The support of the Australian Research Council, through its Discovery and Centres of Excellence programs, is gratefully acknowledged. The authors would also like to acknowledge M. Stevenson, K. Digweed-Lyytikainen, V. Steblina, J. Digweed, J. Zagari and B. Ashton for their assistance with fiber preparation and useful discussions.

#105266 - $15.00 USD Received 12 Dec 2008; revised 18 Jan 2009; accepted 22 Jan 2009; published 29 Jan 2009